Journal of Power Sources 199 (2012) 220–226

Contents lists available at SciVerse ScienceDirect

Journal of Power Sources

journal homepage: www.elsevier.com/locate/jpowsour

Electrochemical and rate performance study of high-voltage lithium-rich composition: $Li_{1.2}Mn_{0.525}Ni_{0.175}Co_{0.1}O_2$

Surendra K. Martha*, Jagjit Nanda**, Gabriel M. Veith, Nancy J. Dudney

Materials Science and Technology Division, Oak Ridge National Laboratory, Oak Ridge, TN 37831, USA

ARTICLE INFO

Article history:
Received 25 August 2011
Received in revised form 5 October 2011
Accepted 6 October 2011
Available online 13 October 2011

Keywords:
Lithium battery
Cathode material
Carbon nanofiber
Rate performance

ABSTRACT

We report electrochemical studies of high voltage cathodes composed of lithium rich "layered-layered" material having the nominal composition $Li_{1.2}Mn_{0.525}Ni_{0.175}Co_{0.1}O_2$, or equivalently $0.6Li[Li_{1/3}Mn_{2/3}]O_2–0.4Li[Mn_{0.3}Ni_{0.45}Co_{0.25}]O_2$. These aspects were investigated by cyclic voltammetry studies in conjunction with electrochemical impedance spectroscopy measurements to understand the redox reactions involving multiple transition metals and their capacity contribution at higher voltages, up to 4.9 V. Further, cathodes with 1.5 wt.% carbon nanofibers added to the $Li_{1.2}Mn_{0.525}Ni_{0.175}Co_{0.1}O_2$ composite electrode showed stable reversible capacities of about 280 mAh g^{-1} when cycled to 4.9 V for more than 100 cycles, and almost a factor of two improvements in the rate performance compared to the electrode composition prepared using conventional composition (7.5% carbon black and 7.5% binder).

Published by Elsevier B.V.

1. Introduction

During the last three decades, a large variety of materials have been synthesized and evaluated as cathode materials for Li-batteries [1–4]. Notable among them is the layered $LiMO_2$ (M = Co, Ni, Mn) compositions which have already found application in rechargeable lithium ion battery technology [1,5]. However, only about 50–60% of the theoretical capacity can be utilized in practical cells because of structural and chemical instabilities associated with deep charge of $Li_{1-x}MO_2 (x > 0.5)$ along with safety issues [1,5]. In order to increase the energy density, recent developments have focused on the lithium rich Li–Ni–Mn–Co oxide compounds that have significantly higher capacities [6–33]. These materials can be represented using either (i) structurally integrated two-component solid solution notations such as xLi_2MnO_3 $(1-x)$ $LiMO_2$ (layered–layered in which the Li_2MnO_3 component is electrochemically activated above 4.4 V *vs.* Li/Li^+) or (ii) standard notation as $Li_{1+y}M_{1-y}O_2$ (M = Mn, Ni, Co) [18–34]. For example, the composition studied here $0.6Li[Li_{1/3}Mn_{2/3}]O_2–0.4Li[Mn_{0.3}Ni_{0.45}Co_{0.25}]O_2$ (hereafter Li-rich MNC) can be alternately expressed as $Li_{1.2}Mn_{0.525}Ni_{0.175}Co_{0.1}O_2$ in the standard notation for such layered compositions [18–34]. Electrodes based on these Li-rich MNC compositions can operate at high anodic potentials of 4.9 V *vs.* Li/Li^+ and provide capacities >250 mAh g^{-1} [18–34]. However, there are still major issues that need to be addressed before these compounds can be consider as high-energy cathodes for Li-ion batteries, especially for electric vehicle application. Notable among them are poor rate capability, high first cycle irreversibility and significant decrease in the discharge voltage plateau with successive cycling [19–34].

The large irreversible capacity loss in the range of 50–100 mAh g^{-1} in the first cycle [17–32] is attributed to the extraction of Li_2O followed by elimination of oxygen ion vacancies from the lattice during first charge, resulting in a lower number of sites for insertion and extraction of Li^+ in the subsequent cycles [16,20]. Further, detailed structural and phase transitions associated with such lithiation–delithiation processes at higher voltage (>4.4 V) are not fully understood yet.

This paper reports the progress in understanding the electrochemical behavior of Li-rich MNC phases cycled to higher voltage (4.9 V) without use of any high voltage electrolytes additives or surface coatings. Further, we report improved rate performance of Li-rich MNC cathodes using carbon nano-fiber as an electrode additive. These results are arranged in three major parts. The first part discusses the characterization of the structure and morphology of Li-rich MNC active material, carbon nanofiber additives and the as fabricated electrodes. The second part reports the electrochemical properties of the Li-rich MNC phase based on cyclic voltammetry and electrochemical impedance spectroscopy. Finally, we report the improvement in the capacity, rate capability and cycle life of Li-rich MNC by addition of a small quantity of carbon nanofiber in the composite electrode.

* Corresponding author. Tel.: +1 865 5746797; fax: +1 865 5746210.
** Corresponding author. Tel.: +1 865 2418361; fax: +1 865 5746210.
E-mail addresses: marthask@ornl.gov (S.K. Martha), nandaj@ornl.gov (J. Nanda).

0378-7753/$ – see front matter. Published by Elsevier B.V.
doi:10.1016/j.jpowsour.2011.10.019

2. Experimental

2.1. Structure and morphology

Li rich MNC powder was obtained from the pilot scale synthesis facility of TODA materials corporation, Japan and detailed characterization studies were performed at Oak Ridge National Laboratory to study their performance and cycle life. Carbon nanofibers (CNFs) manufactured by Applied Sciences Inc., OH, USA. The CNFs were produced by chemical vapor deposition at 3000 °C [35]. Powder X-ray diffraction (XRD) measurements were performed using an XDS 2000 diffractometer (reflection θ–θ geometry, Cu Kα radiation, receiving slit 0.5 mm, scintillation counter, 40 mA, 45 kV) from Scintag, Inc., CA, USA. The diffraction data were collected at 0.025 step widths over a 2θ range from 10° to 90°. The morphology of Li-rich MNC particles, CNFs and electrodes were characterized by Hitachi S-4800 scanning electron microscope (Hitachi High Technologies America, Inc., USA) equipped with a Thermo NORAN system 6 X-Ray microanalysis system supported by a NanoTrace LN-Cooled Si (Li) detector for Energy-dispersive X-ray Spectroscopy (EDX) analysis. The active surface area of the material was measured by the Brunauer, Emmet and Teller (BET) method with a Quantachrome Instrument, FL, USA and the particle size distribution was measured with a laser scattering particle size distribution analyzer (Horiba LA950 from HORIBA Jobin Yvon Inc., NJ, USA). Raman spectroscopy of CNFs was carried out using an Alpha 300 confocal Micro-Raman set up from Witec Instruments, Germany.

2.2. Electrochemical measurements

The electrochemical performance of the cathodes comprising Li-rich MNC as the active mass was evaluated using two and three-electrode coin-type cells (size CR2032, Hohsen Corp., Japan) with a polypropylene membrane separator (type 2325, Celgard, Inc., USA). For comparison, we tested standard electrodes prepared with an N-methylpyrrolidone (NMP) (Aldrich, 99.5% purity) slurry of Li-rich MNC, PVDF (Aldrich), and C-black (CB) (Super P) in wt.% ratio of 85:7.5:7.5 (hereafter 'conventional electrodes') against a slurry of Li-rich MNC, PVDF, C-black and carbon nano-fiber (85:7.5:6:1.5) (hereafter 'CNF-added electrodes'). Both types of electrodes comprised ~10 mg of active Li-rich MNC per cm^2 on Al (Alfa Aesar, 99.99% purity) current collector, which is comparable to commercial electrodes. Lithium foils (purity 99.9%, Alfa Aesar) were used as counter and reference electrodes. The electrolyte solution was 1.2 M $LiPF_6$ in a 1:2 mixture of ethylene carbonate (EC) and dimethyl carbonate (DMC) by weight (battery grade, Novolyte Technologies, USA) with HF and H_2O impurity less than 50 and 20 ppm, respectively. Electrochemical cells were assembled in glove boxes filled with high purity argon. After assembling, the cells were stored at room temperature for about 12 h to ensure complete impregnation of the electrodes and separators with the electrolyte solution. Electrochemical measurements, including impedance and CV in three-electrode coin-type cells, were carried out using Solartron equipment (models 1470E and 1455, Solartron Analytical Ltd., UK) driven by Corrware and ZPlot software (Scribner Associates, USA). Impedance measurements at various cell potentials were carried out in a frequency range between 1 MHz and 5 mHz. For this purpose, the electrodes were charged from open circuit voltage to various potentials and equilibrated for 2 h. Galvanostatic charge–discharge cycling was carried out using a multichannel battery tester (model 4000, Maccor Inc., Tulsa, OK, USA) in two-electrode coin-type cells. Cells were cycled in a potential range of 2.5–4.9 V using a constant current plus constant voltage (CCCV) charge, i.e., charging continued at 4.9 V until the current reached a value corresponding to C/50 value. Discharge was tested by a constant current protocol at various rates to the 2.5 V cutoff potential. Galvanostatic charge–discharge cycling was carried out with at least ten 2-electrode cells and impedance-cyclic voltammetry were conducted with at least two 3-electrode coin-type cells to validate the reproducibility of the results.

3. Results and discussion

3.1. Structure and morphology

The current Li-rich MNC composition is the solid solution of 0.6 Li [$Li_{1/3}Mn_{2/3}$] O_2–0.4Li [$Mn_{0.3}Ni_{0.45}Co_{0.25}$] O_2. Fig. 1a presents XRD data of Li-rich MNC powder corresponding primarily to the R-$NaFeO_2$ structure (O3 structure) [18–21,24,25,27–30]. A weak peak around 21° corresponds to integrated monoclinic Li [$Li_{1/3}Mn_{2/3}$] O_2 phase (C2/m), originating from the ordering of Li^+ ion in the transition metal layer [27–29]. SEM images of Li-rich MNC. SEM images of the Li-rich MNC particles are presented in Fig. 1b. As seen in image, the aggregated secondary particles are spherical in shape having a diameter ranging between 5 and 15 μm. The secondary particles comprise of primary particles having sizes between 80 and 110 nm (Fig. 1c). For the studied composition, $Li_{1.2}Mn_{0.525}Ni_{0.175}Co_{0.1}O_2$, the particle size distribution obtained from laser diffraction method (not shown here) was found to be as follows: d (0.1) = 7.3, d (0.5) = 11.6, d (0.9) = 17.1 μm. This signifies the average secondary particle size is ~12 μm (d (0.5) = 11.6).

The active surface area of the material were estimated to be 3.2 $m^2\,g^{-1}$ by the Brunauer, Emmet and Teller (BET) method and the tap density of material was about 1.74 g cm^{-3}. Elemental analysis by energy dispersive analysis of X-rays shows the ratio between Mn:Ni:Co to be 0.525:0.175:0.1 in agreement with the compositional analysis of the supplier. Fig. 1d presents the SEM image of the composite electrode having 7.5% each of CB and PVDF and 85% of Li-rich MNC particles, which are mostly covered with CB and PVDF particles. Fig. 2a shows the SEM image of CNFs. They appear to be thread-like structures with an outer diameter of 100–200 nm and a hollow core typically about 1/2–2/3 of the total fiber diameter. Fig. 2b presents the Raman spectrum of the CNFs, reflecting the strong graphitic nature of the material. The strong band at 1590 cm^{-1} mainly corresponds to the G-line associated with the optically allowed E_{2g} vibration of the graphitic structure. The peak around 1361 cm^{-1} mainly corresponds to the D-line associated with disordered carbon vibrations. The strong graphitic peak at 1590 cm^{-1} followed by a weak defect (D) band suggests that the fibers are highly conducting with carbon atoms mainly having sp^2 type bond geometry [36]. The second order peaks at 2700 and 2450 cm^{-1} are marked by an asterisk in Fig. 2b. Fig. 2c shows the SEM image of the composite electrodes with 7.5% of PVDF, 6% CB, 1.5% CNFs Li-rich MNC particles demonstrating the CNF forming a conducting network around the secondary aggregates.

3.2. Electrochemical studies

3.2.1. Cyclic voltammetry

Fig. 3 presents typical initial and steady state cyclic voltammograms (CVs) of CNF-added composite electrodes comprising Li-rich MNC as the active mass with different charge cutoff potentials, obtained at a scan rate of 100 μV s^{-1} and at 25 °C. As previously reported for layered Li–Ni–Mn–Co system (e.g., $LiNi_{1/3}Mn_{1/3}Co_{1/3}O_2$ or $LiNi_{0.5}Mn_{0.3}Co_{0.2}O_2$ and similar compositions), the redox peaks at 3.85/3.6 V corresponds to Ni^{2+}/Ni^{4+} redox reaction in the Li–Ni–Mn–Co oxide lattice [5,37] and hence it is expected to be same for the Li-rich MNC system as well. The high redox potential 4.5 V/4.3 in Li-rich MNC is due to the partial redox contribution from Co^{3+} to Co^{4+} that corresponds to the second electron transfer. The CVs of layered Li–Ni–Mn–Co system does not

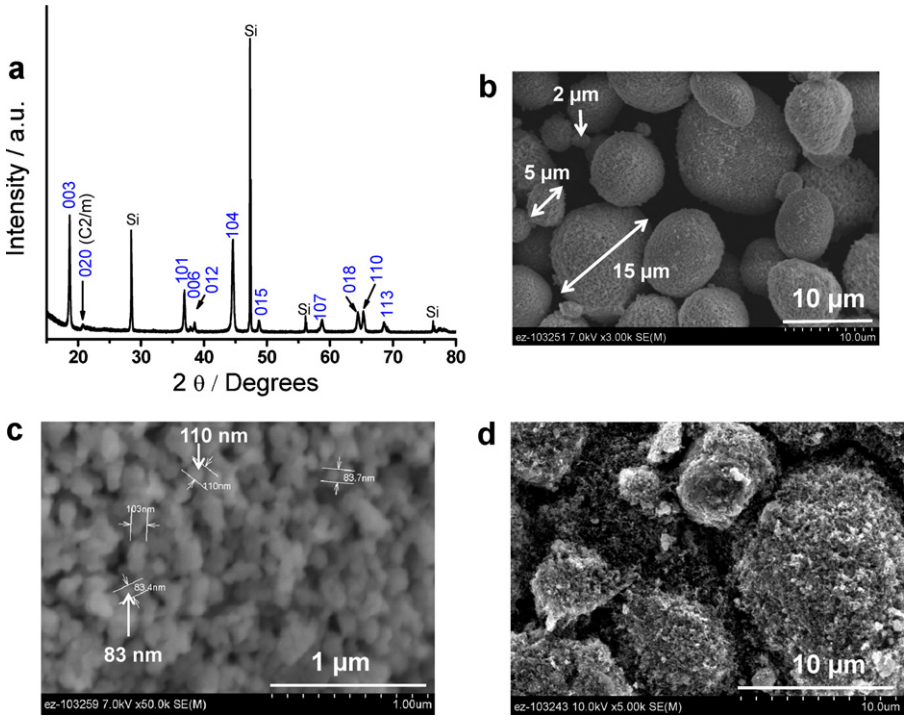

Fig. 1. (a) XRD patterns of the $Li_{1.2}Mn_{0.525}Ni_{0.175}Co_{0.1}O_2$ (Li-rich MNC) particles. Miller indexes of the main reflections are indicated. Si powder was added as a reference to Li-rich MNC powder. The silicon peaks are marked as Si. (b) SEM image of bare Li-rich MNC particles (3000×; scale bars are 10 μm), (c) zoomed image of a secondary Li-rich MNC particle comprise of primary particles having sizes between 80 and 110 nm (50,000×; scale bars are 1 μm) and (d) SEM image of the composite cathode (termed as conventional cathode) containing 85% Li-rich MNC particles – 7.5% PVDF – 7.5% CB (5000×; scale bars are 10 μm).

usually show Co^{3+}/Co^{4+} redox peaks as they are normally cycled below 4.5 V. Parallel study (data not presented here) shows the capacity measured in the potential range of 2.5–4.5 V shows that only Li $[Mn_{0.3}Ni_{0.45}Co_{0.25}]$ O_2 is activated in this region (which is also seen in the scan 1 between 2.5 and 4.5 V of Fig. 3). Charging to 4.9 V, results in the electrochemical activation of the Li_2MnO_3 component by its decomposition to Li_2O and MnO_2. So this peak at 3.0 V becomes apparent after charging to 4.9 V and can be ascribed to the oxidation (at 3.2 V – anodic delithiation) and reduction (at 3.0 – cathodic lithiation) of the manganese ions Mn^{3+}/Mn^{4+} that

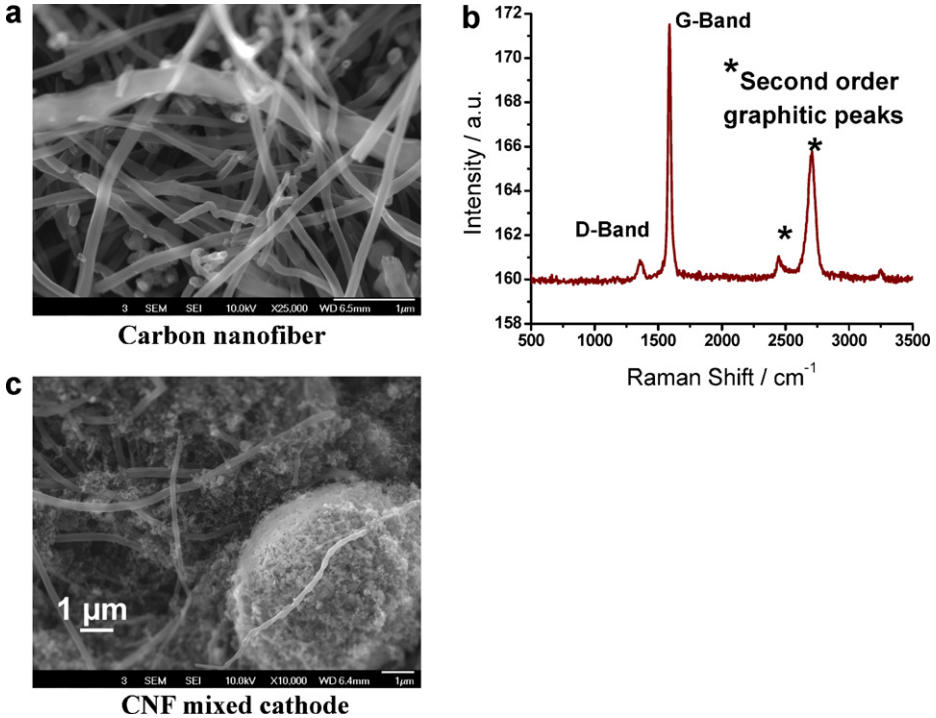

Fig. 2. (a) SEM image of carbon nanofibers (CNFs), (b) Raman spectrum of CNFs indicating D, G bands and second order graphitic peaks. (c) SEM image of the CNF-added composite cathode containing 85% Li-rich MNC particles-7.5% PVDF-6% CB, 1.5% CNFs (10,000×; scale bars are 1 μm).

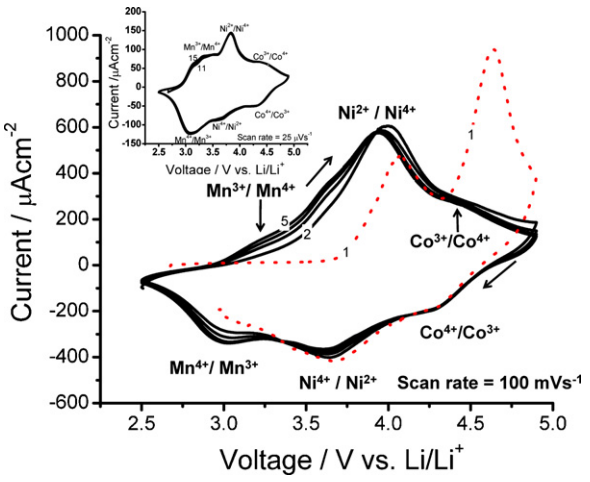

Fig. 3. Cyclic voltammograms (100 μV s^{-1}) measured with CNF-added lithium rich MNC composite electrodes at cutoff potential between 2.5 and 4.9 V (cycles 1–5) in EC-DMC 1:2/$LiPF_6$ 1.2 M solution at 25 °C. Data between 2.9 V and 2.5 V during first cycle were noisy and hence deleted. The inset is the CVs (cycles between 11 and 15) at 25 μV s^{-1} measured with CNF-added lithium rich MNC electrodes clearly indicating Mn, Ni, Co redox species.

may take place in the electrochemical reaction after the Li_2MnO_3 component has been electrochemically activated [18–21,30]. The large irreversible capacity (later shown in Fig. 5b) is aptly reflected in the first cycle CV after 4.4 V by the large anodic peak. Slow scan CVs (cycles 11–15) at 25 μV s^{-1} for CNF-added Li-rich composite electrodes presented in the inset to Fig. 3 clearly indicating Mn, Ni and Co redox behaviors. The successive CVs after the first cycle are overlapping (cycles 2–5 and 11–15) showing no loss of capacity or net electrochemical activity within the desired voltage range. This high voltage stability is further supported by the galvanostatic cycling experiments at various operating potentials, as described in the subsequent section.

3.2.2. Electrochemical impedance spectroscopy (EIS)

Fig. 4 shows impedance spectra, presented as Nyquist plots, of CNF-added Li-rich MNC composite electrodes at 25 °C measured at various equilibrium potentials: (a) 3.0 V, 3.5 V, 4.0 V; (b) 4.0 V, 4.2 V, 4.4 V, 4.5 V; (c) 4.5 V, 4.6 V, 4.8 V, 4.9 V, 5.0 V; and (d) zoomed image of 4.8 V, 4.9 V, 5.0 V as indicated. They are presented in four different Nyquist plots for better clarity instead of one plot. The overall EIS responses depend strongly on electrode potential or state of charge (SoC). The impedance spectra of the electrodes contain (i) a high to medium frequency feature that appears like a flat semicircle most likely originating from the resistance due to the surface passivation film and (ii) a medium to low frequency semicircle, which related to the interfacial charge-transfer resistance. The surface layer resistance (resistance of Li^+ migration through the surface films that are formed on all lithiated transition metal oxide cathodes) decreases from open circuit voltage until 4.0 V and it is almost the same for all other voltages >4.0 V. The charge transfer resistance R_{CT} decreases with Mn and Ni oxidation (from open circuit voltage until 4.0 V) and increases after 4.2 V. The activation of the Li_2MnO_3 component by its decomposition to Li_2O and MnO_2 starts above 4.2 V. The increase in R_{CT} can be ascribed either to the passivating effect of MnO_2 on the electrode surface after 4.2 V or to the structural rearrangements of the Li-rich MNC electrodes due to oxygen loss from lattice [30]. The low-frequency straight line at voltages between 3.0 V and 4.2 V, which resembles a 'Warburg'-type element, belong

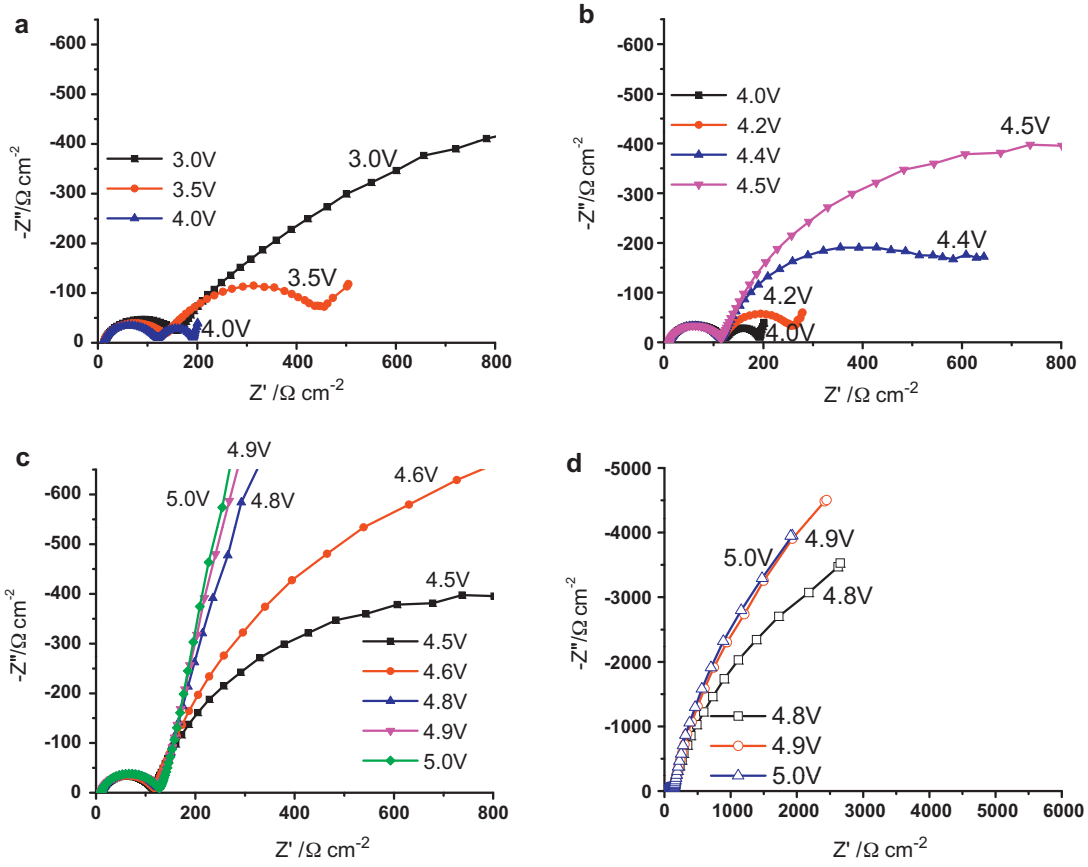

Fig. 4. A family of impedance spectra, represented as Nyquist plots, of CNF-added Li-rich MNC composite electrodes at 25 °C measured at various equilibrium potentials (a) 3.0, 3.5, 4.0 V, (b) 4.0, 4.2, 4.4, 4.5 V, (c) 4.5, 4.6, 4.8, 4.9, 5.0 V and (d) zoomed image of 4.8, 4.9, 5.0 V as indicated at T = 25 °C during Li-deintercalation processes.

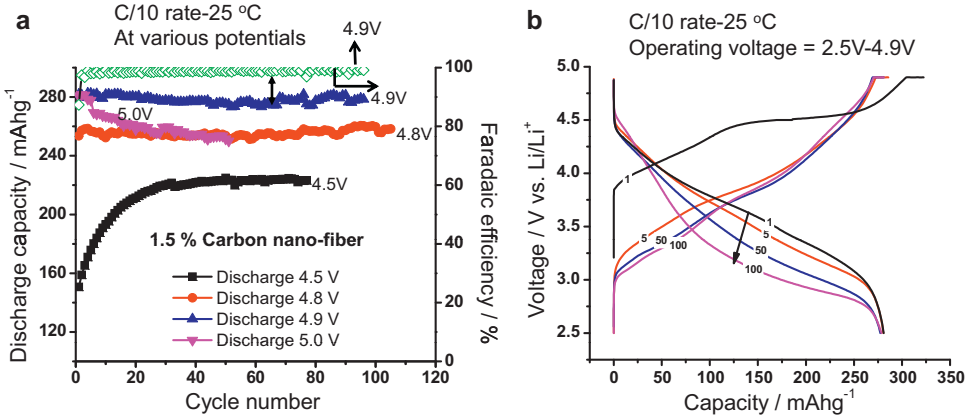

Fig. 5. (a) Discharge capacity data at various potentials (as indicated) of CNF-added Li-rich MNC composite electrodes at C/10 rate, in EC-DMC 1:2/$LiPF_6$ 1.2 M solutions (coin-type cell, T = 25 °C). Cycling protocol was constant current–constant voltage providing potentiostatic steps at desired higher cut-off potential until the current reach value of C/50. The lower cut off potential was 2.5 V *vs.* Li/Li^+. The faradaic efficiency during operation between 2.7 and 4.9 V is also presented in the right *Y*-axis. (b) Voltage profiles of CNF-added Li-rich MNC composite electrodes measured galvanostatically at C/10 rate during 100 cycles (cycle numbers are indicated in the voltage profile) at 25 °C. The cycling protocol was same as above.

to the solid-state diffusion of Li ions within the solid active mass. After 4.2 V the 'Warburg'-component disappears and spectra looks like only two semi circles (Fig. 4c and d). The Mn^{3+}/Mn^{4+} redox peaks at 3.0 V are reversible after electrochemical activation of the Li_2MnO_3 component by its decomposition to Li_2O and MnO_2. The CVs of Li-rich MNC electrodes indicate that these electrodes can be cycled at high anodic potentials up to 4.9 V. The increase in R_{CT} is either due to the passivating effect of MnO_2 on the electrode surface after 4.2 V or to the structural rearrangements of the Li-rich MNC electrodes due to oxygen loss from lattice.

3.3. Capacity and rate performance

Electrochemical cycling data are presented in Fig. 5a of four different cells (C/10 rate at 25 °C) for CNF-added Li-rich MNC composite electrodes in galvanostatic mode when charged to various cut-off potentials (4.5, 4.8, 4.9 and 5.0 V). In all these experiments, discharge was carried out purely galvanostatically, while charging was performed using a CC–CV protocol (see Section 2). Similar to the CV results, when these cells are cycled between 2.5 and 4.5 V, an initial capacity of 160 mAh g^{-1} could be achieved. However, with increase in the number of cycles the capacity increases, and reversible capacities up to 220 mAh g^{-1} could be achieved for these electrodes within this potential range. As already mentioned in the literature [18–23,30], Li_2MnO_3 is activated above 4.4 V. So the gradual increase in capacity can be attributed to the slow activation of a small amount of Li_2MnO_3 component at 4.5 V. Further charging to 4.8 V and above results in the complete activation of the Li_2MnO_3 component leading to formation of Li_2O and MnO_2. Increasing the cycling window from 4.8 V to 4.9 V, results a 10% increase in capacity for these CNF-added Li-rich MNC composite electrodes. Maximum capacity of 280 mAh g^{-1} can be achieved for the CNF-added Li-rich MNC composite electrodes at cut-off potential of 4.9 V at C/10 rate. Increasing the upper cut-off potential to 5.0 V, showed no further increase in capacity. The capacities at high anodic potentials 4.9 V and 5.0 V were identical for few initial cycles, but the discharge capacities substantially decrease after 5 cycles indicating electrolyte instability at high anodic potentials of 5.0 V. A 10% decrease in capacity was observed at the end of 50 cycles when the electrodes are cycled between 2.5 and 5.0 V. During their operation between 2.5 and 4.9 V, the cells retain their capacity for 100 cycles with minor loss (0.01% per cycle) in capacity. Faradaic efficiency close to 99.95% was observed for these cells during operation for the first 100 cycles.

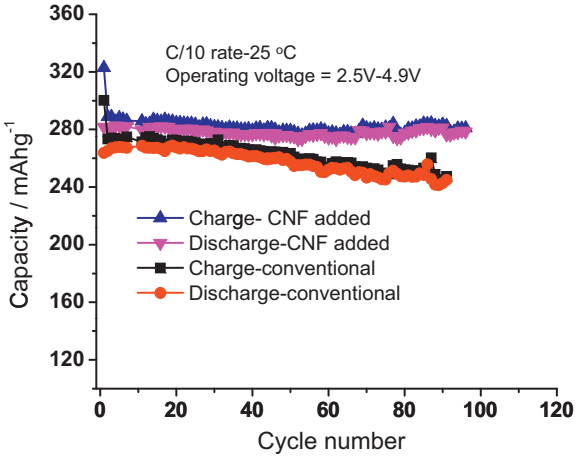

Fig. 6. Cycling behavior at C/10 rates of charge–discharge for the CNF-added and conventional Li-rich MNC composite electrodes (as indicated) in the potential range 2.5–4.9 V, in EC-DMC 1:1/$LiPF_6$ 1.2 M solutions at 25 °C. The cycling protocol was similar to that of Fig. 5.

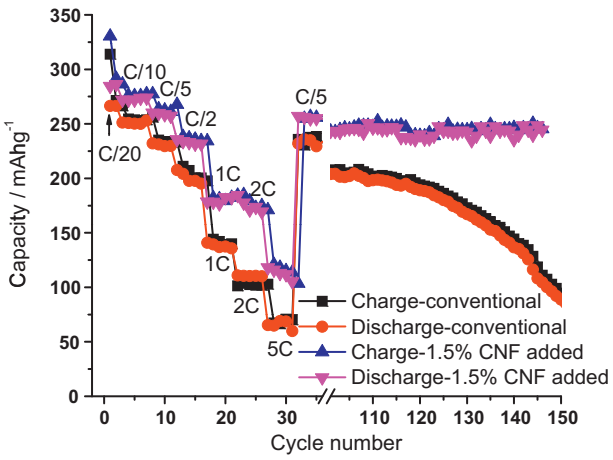

Fig. 7. Comparison of rate capabilities (charge/discharge capacity *vs.* rates) for conventional and CNF-added Li-rich MNC composite electrodes measured galvanostatically at various rates (as indicated) at 25 °C. The cycling protocol was similar to that of Fig. 5.

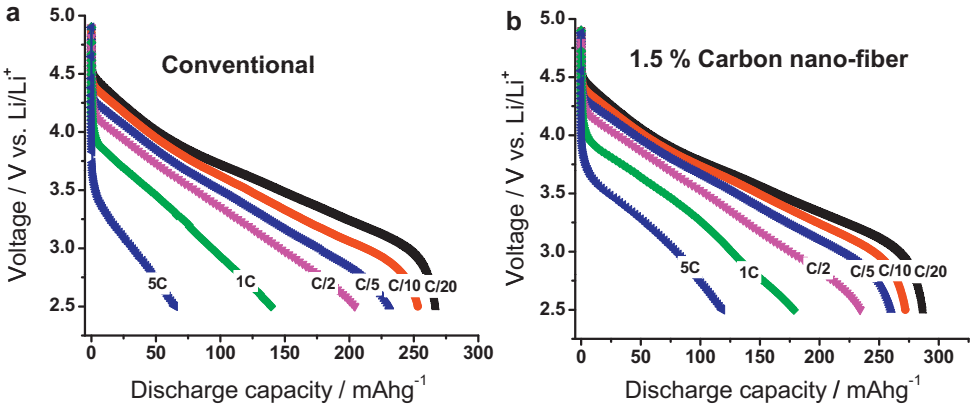

Fig. 8. Voltage profiles of (a) conventional and (b) CNF-added Li-rich MNC composite electrodes measured galvanostatically at various discharge rates (as indicated) at 25 °C. The cycling protocol was similar to that of Fig. 5.

Fig. 5b presents the voltage profiles for the CNF-added Li-rich MNC composite electrodes at C/10 rate during 100 cycles between 2.5 and 4.9 V. The first charge voltage profile clearly shows the high voltage plateaus at 4.5 V. In previous reports by MacNeil et al. [38] and Armstrong et al. [16], this excess capacity at 4.5 V is attributed to extraction of Li_2O from the lithium rich layers with a concomitant loss of oxygen. In related work, Hong et al. reported the excess capacity originating at the 4.5 V plateau resulted from the hybridization of O^{2-} 2p orbital and Mn^{4+} −3d orbital [39].

As shown in charge–discharge profiles *vs.* the cycle number (Fig. 5b), with successive cycling the CNF-added Li-rich MNC composite electrodes retains high capacity along 100 cycles but the discharge profiles move to lower voltage plateaus showing significant loss of energy. The high voltage plateau decreased by ~50% at the end of 100 cycles. The origin of such rapid drop in the discharge voltage profile is at present not fully understood but could be related to the gradual change to a spinel-like structure [21]. It should be noted that these electrodes deliver capacity of 175 mAh g^{-1} in the first cycle above 3.5 V and this has been reduced to 75 mAh g^{-1} at the same voltage after 100 cycles. However, upon full discharge to 2.5 V, these electrodes demonstrate only minor loss in capacity (1% loss) during 100 cycles as most of the capacity is delivered at lower potentials.

Fig. 6 presents cycling performance of CNF-added compared to conventional Li-rich composite electrodes at C/10 rate. During the extended cycling, the CNF-added Li-rich MNC electrodes barely lose any capacity (1% capacity loss) for 100 cycles whereas conventional electrodes have lost almost 10% of their original capacity at the end of 100 cycles. This can be attributed to the high conductivities of CNFs, which makes a good contact along the spherical MNC particles. Looking now at the first cycle charge, both cathodes show an anomalously high capacity of about 325 mAh g^{-1}. The irreversible capacity at the first cycle for the CNF-added Li-rich composite electrodes was about 16–18% at C/10 rate (Figs. 5b and 6). Recent literature reports indicate the origin of such anomalous first cycle charge capacity could be due to products of electrolyte oxidation reactions at high anodic potentials or possible Li_2O formation (with subsequent release of oxygen) during electrochemical activation of Li_2MnO_3 [16,20,21,30].

The rate capability data for conventional and CNF-added Li-rich MNC composite electrodes, presented in Fig. 7, show significant improvement with the CNF-added electrodes. About 7–10%, higher capacity can be achieved at low discharge rates (<C/2) and 25–30% higher capacity can be achieved for CNF-added electrode than conventional electrodes at high discharge rates (>1C). Typically, the CNF-added Li-rich composite electrodes studied herein exhibit an initial discharge capacity of 280–282 mAh g^{-1} at low rates (C/20), 260 mAh g^{-1} at C/5 rate and maintain high capacity retention (>99.9%) upon cycling at various rates up to 5C rates (and back to low rates) for both the conventional and CNF-added electrodes. Only 60 mAh g^{-1} capacity can be obtained for conventional Li-rich MNC composite electrodes at 5C rate, whereas CNF-added Li-rich MNC composite electrodes deliver almost the double capacity (120 mAh g^{-1}) of conventional electrodes at similar rate. It is to be noted that the electrodes are of comparable mass per cm^2 of commercial electrodes. Still the high rate performance of the electrodes at 5C and higher rates are not impressive. The poor rate capability could be related to the low electronic conductivity associated with the Mn^{4+} ions or the thick solid–electrolyte interfacial (SEI) layer formed by a reaction of the cathode surface with the organic electrolytes [24,27]. In addition, poor rate performance could be due to poor solid-state diffusion of Li-rich MNC. The conventional electrodes start declining capacity very rapidly after 120 cycles where as CNF-added Li-rich MNC electrodes maintain the capacity. These results clearly show that the CNFs maintain a good electrical contact along the Li-rich MNC particles; and retain good electrochemical performance during long cycling. The discharge voltage profiles of CNF-added and the conventional Li-rich MNC composition shown in Fig. 8a and b exhibit similar sloping pattern except that CNF composition has better capacity retention at higher rates.

The irreversible capacity at the first cycle for the CNF-added and conventional Li-rich MNC composite electrodes were identical, about 16–18% at C/10 rate. 25–30% higher capacity can be achieved for CNF-added electrode over conventional electrodes at high discharge rates (>1C). Maximum capacity of 280 mAh g^{-1} can be achieved for the CNF-added Li-rich MNC composite electrodes at cut-off potential of 4.9 V at C/10 rate. Presumably, CNFs maintain a good electrical contact or network between the Li-rich MNC particles; and retain good electrochemical performance during long cycling.

4. Conclusions

In this study, we have reported detailed electrochemical investigation of the Li rich MNC composition to understand the origin of the higher capacity during the first charge cycle and the subsequent electrochemical behavior upon high voltage cycling (4.9 V). The rate performance of the Li rich MNC composition is improved by almost two fold upon addition of about 1.5 wt.% highly graphitic carbon nanofibers compared to the standard electrode composition (7.5% carbon black and 7.5% PVDF). Reversible capacities close to the 280 mAh g^{-1} at a cut off potential of 4.9 V can be achieved

for the electrodes. These CNF additive electrodes behave reversibly for hundreds of cycles with only minor loss in capacity. The gradual decrease of the high voltage discharge plateau with cycle number signifies structural and compositional changes undergo upon high voltage electrochemical cycling.

Acknowledgments

Materials used in this study were supplied courtesy of Max L. Lake (Applied Sciences, Inc.), carbon nano fibers and Toda Materials Corporation, Japan for the lithium rich MNC composition. This work is funded by the Assistant Secretary for Energy Efficiency and Renewable Energy, Office of Vehicle Technologies of the U.S. Department of Energy. GMV acknowledges support from the Office of Basic Energy Sciences, Materials Sciences and Engineering Division, U.S. Department of Energy. Oak Ridge National Laboratory is managed by UT-Battelle, LLC, for the U.S. Department of Energy under contract no. DE-AC05-00OR22725.

References

[1] M.S. Whittingham, Chem. Rev. 104 (2004) 4271–4430.
[2] J.B. Goodenough, A.K. Padhi, K.S. Nanjundaswamy, C. Masquelier, Cathode materials for secondary (rechargeable) lithium batteries, US Patent 5910382 (1999).
[3] A.S. Aricò, P. Bruce, B. Scrosati, J-M. Tarascon, W.v. Schalkwijk, Nat. Mater. 4 (2005) 366–377.
[4] S.K. Martha, J. Grinblat, O. Haik, E. Zinigrad, T. Drezen, J.H. Miners, I. Exnar, A. Kay, B. Markovsky, D. Aurbach, Angew. Chem. Int. Ed. 48 (2009) 8559–8563.
[5] S.K. Martha, H. Sclar, Z. Framovich, D. Kovacheva, N. Saliyski, Y. Gofer, P. Sharon, E. Golik, B. Markovsky, D. Aurbach, J. Power Sources 189 (2009) 248–255.
[6] K. Numata, C. Sakaki, S. Yamanka, Solid State Ionics 117 (1999) 257–263.
[7] J.-S. Kim, C.S. Johnson, M.M. Thackeray, Electrochem. Commun. 4 (2002) 205–209.
[8] Z. Lu, J.R. Dahn, J. Electrochem. Soc. 149 (2002) A815–A822.
[9] J.-H. Kim, Y.-K. Sun, J. Power Sources 119–121 (2003) 166–170.
[10] Y.J. Park, X. Wu, Y.-S. Hong, K.S. Ryu, S.H. Chang, Solid State Ionics 175 (2004) 305–309.
[11] L. Zhang, K. Takada, N. Ohta, L. Wang, T. Sasaki, M. Watanabe, Mater. Lett. 58 (2004) 3197–3200.
[12] K.S. Park, M.H. Cho, S.J. Jin, C.H. Song, K.S. Nahm, J. Power Sources 146 (2005) 281–286.
[13] P.S. Whitfield, S. Niketic, I.J. Davidson, J. Power Sources 146 (2005) 617–621.
[14] M.M. Thackeray, C.S. Johnson, J.T. Vaughey, N. Li, S.A. Hackney, J. Mater. Chem. 15 (2005) 2257.
[15] C.S. Johnson, N. Li, J.T. Vaughey, S.A. Hackney, M.M. Thackeray, Electrochem. Commun. 7 (2005) 528–536.
[16] A.R. Armstrong, M. Holzapfel, P. Novàk, C.S. Johnson, S.-H. Kang, M.M. Thackeray, P.G. Bruce, J. Am. Chem. Soc. 128 (2006) 8694–8698.
[17] S.J. Jin, K.S. Park, M.H. Cho, C.H. Song, A.M. Stephan, K.S. Nahm, Solid State Ionics 177 (2006) 105–112.
[18] S.-H. Park, S.-H. Kang, C.S. Johnson, K. Amine, M.M. Thackeray, Electrochem. Commun. 9 (2007) 262–268.
[19] S.-H. Kang, P. Kempgens, S. Greenbaum, A.J. Kropf, K. Amine, M.M. Thackeray, J. Mater. Chem. 17 (2007) 2069–2077.
[20] M.M. Thackeray, S.-H. Kang, C.S. Johnson, J.T. Vaughey, R. Benedek, S.A. Hackney, J. Mater. Chem. 17 (2007) 3112–3125.
[21] C.S. Johnson, N. Li, C. Lefief, J.T. Vaughey, M.M. Thackeray, Synth. Chem. Mater. 20 (2008) 6095–6106.
[22] G.-Y. Kim, S.-B. Yi, Y.J. Park, H.-G. Kim, Mater. Res. Bull. 43 (2008) 3543–3552.
[23] J. Cabana, S.-H. Kang, C.S. Johnson, M.M. Thackeray, C.P. Grey, J. Electrochem. Soc. 156 (2009) A730–A736.
[24] Q.Y. Wang, J. Liu, A.V. Murugan, A. Manthiram, J. Mater. Chem. 19 (2009) 4965–4972.
[25] A. Ito, D. Li, Y. Sato, M. Arao, M. Watanabe, M. Hatano, H. Horie, Y. Ohsawa, J. Power Sources 195 (2010) 567–573.
[26] X. Zhang, W.J. Jiang, A. Mauger, Qili, F. Gendron, C.M. Julien, J. Power Sources 195 (2010) 1292–1301.
[27] J. Liu, A. Manthiram, J. Mater. Chem. 20 (2010) 3961–3967.
[28] J. Liu, B. Reeja-Jayan, A. Manthram, J. Phys. Chem. C 114 (2010) 9528–9533.
[29] J. Liu, Q. Wang, B. Reeja-Jayan, A. Manthiram, Electrochem. Commun. 12 (2010) 750–753.
[30] F. Amalraj, D. Kovacheva, M. Talianker, L. Zeiri, J. Grinblat, N. Leifer, G. Gobes, Markovsky, D. Aurbach, J. Electrochem. Soc. 157 (2010) A1121–A1130.
[31] D. Kim, J. Gim, J. Lim, S. Park, J. Kim, Mater. Res. Bull. 45 (2010) 252–255.
[32] J. Li, R. Klöpsch, M.C. Stan, S. Nowak, M. Kunze, M. Winter, S. Passerini, J. Power Sources 196 (2011) 4821–4825.
[33] N. Yabuuchi, K. Yoshii, S.-T. Myung, I. Nakai, S. Komaba, J. Am. Chem. Soc. 133 (2011) 4404–4419.
[34] S.-H. Kang, W. Lu, K.G. Gallagher, S.-H. Park, V.G. Pol, J. Electrochem. Soc. 158 (2011) A936–A941.
[35] G.G. Tibbetts, M.L. Lake, K.L. Strong, B.P. Rice, Compos. Sci. Technol. 67 (2007) 1709–1718.
[36] F. Tuinstra, J.L. Koenig, J. Compos. Mater. 4 (1970) 492–499.
[37] H. Sclar, D. Kovacheva, E. Zhecheva, R. Stoyanova, R. Lavi, G. Kimmel, J. Grinblat, O. Girshevitz, F. Amalraj, O. Haik, E. Zinigrad, B. Markovsky, D. Aurbach, J. Electrochem. Soc. 156 (2009) A938–A948.
[38] D.D. MacNeil, Z. Lu, J.R. Dahn, J. Electrochem. Soc. 149 (2002) A1332–A1336.
[39] Y.-S. Hong, Y.J. Park, K.S. Ryu, S.H. Chang, Solid State Ionics 176 (2005) 1035–1042.